Optics and Lasers in Engineering 50 (2012) 883–886

Contents lists available at SciVerse ScienceDirect

Optics and Lasers in Engineering

journal homepage: www.elsevier.com/locate/optlaseng

Pulsed laser micromachining of Mg–Cu–Gd bulk metallic glass

Hsuan-Kai Lin [a], Ching-Jen Lee [b,*], Ting-Ting Hu [b], Chun-Han Li [c], J.C. Huang [b]

[a] Graduate Institute of Materials Engineering, National Pingtung University of Science and Technology, Pingtung 91201, Taiwan
[b] Department of Materials and Optoelectronic Science, Center for Nanoscience and Nanotechnology, National Sun Yat-Sen University, Kaohsiung 804, Taiwan
[c] Laser Application Technology Center/Industrial Technology Research Institute South (ITRI South), Liujia Shiang, Tainan 734, Taiwan

ARTICLE INFO

Article history:
Received 5 November 2011
Received in revised form
12 December 2011
Accepted 4 January 2012
Available online 2 February 2012

Keywords:
Metallic glasses
Laser processing
Magnesium

ABSTRACT

Micromachining of Mg-based bulk metallic glasses (BMGs) is performed using two kinds of pulsed nanosecond lasers: a 355 nm ultraviolet (UV) laser and a 1064 nm infrared (IR) laser. Precision machining on the micrometer scale and the preservation of amorphous or short-range order characteristics are important for the application of BMGs in micro-electro-mechanical systems. A higher micromachining rate is achieved using the UV laser than using the IR laser due to a better absorption rate of the former by Mg-based BMGs and a higher photon energy. The cutting depth of Mg-based BMGs ranges from 1 to 80 μm depending on the laser parameters. By appropriate adjustment of the laser power and scan speed, successful machining of the Mg-based BMG with preservation of the amorphous phase is achieved after the laser irradiation process. Short-pulse laser cutting represents a suitable alternative for machining of micro components.

1. Introduction

Bulk metallic glasses (BMGs) are disordered materials that lack the periodicity of crystalline structures. BMGs exhibit many exceptional physical, chemical, and mechanical properties that differ markedly from those of crystalline metals, and thus, BMGs have attracted considerable attention as structural materials [1–4]. It is difficult to fabricate nanometer-sized (on the scale of several hundred nanometers) components using crystalline alloys given that their grain size falls in the range 10–100 μm. However, the short-range atom clusters and viscous flow in the super-cooled liquid region of BMGs allow the formation of BMGs with sizes as low as 10–100 nm [3]; thus, BMGs exhibit good potential as materials for micro-electro-mechanical systems and functional applications.

Conventional cutting tools [5,6] and focused ion beam (FIB) milling [7] offer certain advantages for the machining of micro components made from BMGs. For example, FIB allows precision machining on the nanometer scale and preserves amorphous or short-range order characteristics. Nonetheless, its relatively low machining rate and high cost make it unsuitable for mass production. With the development of laser micromachining techniques, diode-pumped Q-switched lasers have been applied to the patterning of various materials, including ceramics, metals, polymers, and semiconductors [8–13]. The morphology and microstructure of the patterned materials depend on the laser parameters. The traditional laser machining process employing long-pulse (ms) lasers is not appropriate for the manufacture of micro components, given that shorter pulses are needed to minimize crystallization [14]. The use of ultrashort-pulse (fs or ps) lasers is desirable because the short pulse preserves the amorphous characteristics of metallic glasses (MGs) [10,12,13,15] after laser ablation due to the fact that the irradiation time during a single pulse is shorter than electron cooling and lattice heating times, which prevents materials from accumulating heat and thus suppresses microstructural changes. However, the high cost of ultrashort-pulse lasers has limited their application to laboratory research. Consequently, current industrial applications mainly employ short-pulse lasers with nanosecond pulse rates. Short-pulse laser cutting is a good choice for machining of micro components given that the spot size of the laser beam can be reduced to several micrometers via an optical system.

There are three main BMG alloy systems with a low glass transition temperature (T_g). These can be classified as Au-based [16], Mg-based [17,18], and Ce-based [19] MGs. Of these three systems, the Mg-based MGs are most suitable for industrial purposes given that the use of Au-based MGs are limited by their high cost and the high oxidation rate of Ce-based MGs make them unsuitable for mass production. Mg-based MGs have a low T_g (130–140 °C), close to that of poly(methyl methacrylate), meaning that they have good forming ability and good strength. Therefore, to minimize the heat-affected zone (HAZ) and crystallization and maintain an amorphous structure in BMGs, the present study investigates the effects of various laser parameters

* Corresponding author. Tel.: +886 7 5254070; fax: +886 7 5254099.
E-mail address: leechingjen@gmail.com (C.-J. Lee).

0143-8166/$ - see front matter © 2012 Elsevier Ltd. All rights reserved.
doi:10.1016/j.optlaseng.2012.01.003

such as laser fluence and scan speed on the micromachining of a Mg–Cu–Gd ($Mg_{65}Cu_{25}Gd_{10}$) BMG using 355 nm ultraviolet (UV) and 1064 nm infrared (IR) pulsed nanosecond lasers.

2. Experimental procedure

A Mg-based BMG alloy comprising $Mg_{65}Cu_{25}Gd_{10}$ (atomic %) was selected as the test material. The alloy was injection-casted into a water-cooled Cu mold with an internal cylindrical-shaped cavity measuring 3 mm in diameter. X-ray diffraction (XRD) and differential scanning calorimetry (DSC) measurements were performed to verify the amorphous nature of the cast alloy. The 3 mm-diameter BMG rod was sliced into disks of 1.5 mm height using a diamond cutter, and the disks were subsequently ground using SiC papers of grades ranging from 1200 to 4000. Finally, the disk surfaces were polished to a mirror finish with a diamond polish paste with grit sizes ranging from 0.25 to 1 μm, prior to the laser micromachining.

The system for laser micromachining consisted of two laser sources with a stability greater than 90%, a scanner (Scanlab), and an XYZ stage. The laser experiments were performed using a UV laser (Coherent AVIA 355–7000) with a wavelength of 355 nm, a repetition rate of 40 kHz, and a pulse duration of 30 ns, and an IR laser (SPI SP-20P) with a wavelength of 1064 nm, a repetition rate of 25 kHz, and pulse duration of 30 ns. Micromachining of the Mg-based BMG was carried out at a laser power of 3–6 W; the scan speed was varied from 30 to 400 mm/s.

To increase the resolution of the micromachined pattern, the size of the laser spot was decreased. The diameter of the laser spot, D_0, is expressed as:

$$D_0 = 1.22 \times \left(\frac{\lambda \times F}{n \times W_d}\right) \times M^2 \quad (1)$$

where λ is the laser wavelength, F the focal length, n the refractive index, W_d the diameter of the incident laser, and M^2 the laser-quality factor. Eq. (1) indicates that the diameter of the laser beam is directly proportional to the wavelength and focal length. For the experiment, the spot size was 40 μm. The absorption spectrum and crystalline structure of the Mg-based BMG specimens before and after micromachining were measured using grazing incidence in-plane X-ray diffraction, a surface profiler (α-step, Tencor), and a UV–vis-IR spectrophotometer (Jasco V-750). The morphology and component ratios of machined samples were examined by scanning electron microscopy and FIB.

3. Results and discussion

To examine the rate of absorption of various irradiation wavelengths by the Mg-based BMG specimens, the reflectivity of the disk specimens was measured using a UV–vis-IR spectrophotometer. Fig. 1 shows the reflectivity of the Mg-based BMG specimens for wavelengths in the range 200–1400 nm. Due to a change in the incident light source, the reflectivity spectrum exhibits discontinuities at wavelengths of 350 and 900 nm. Reflectivities of 23% and 55% were obtained at 355 and 1064 nm, respectively. From the equation of absorption, $(A)=1$ reflectivity (R), the absorption rate of Mg-based BMG at a wavelength of 355 nm is found to be 1.7 times higher than that at 1064 nm.

Table 1 lists the micromachining depth, measured using a surface profiler, of Mg-based BMG specimens obtained using various laser cutting parameters. For the UV laser with a fluence of 6 J/cm^2, increasing the scan speed from 30 to 300 mm/s resulted in a decrease in the cutting depth from 30 to 7.2 μm.

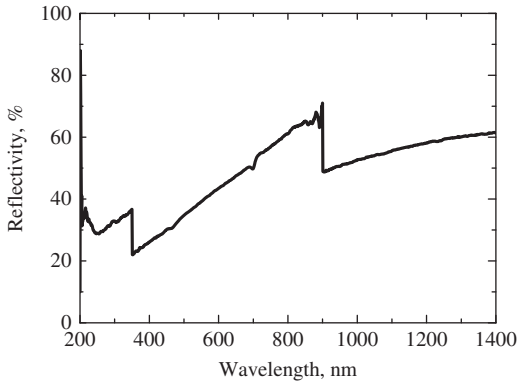

Fig. 1. Optical reflectivity spectra for wavelengths from 200 to 1400 nm for Mg-based BMG.

Table 1
Micromachining depths of Mg-based BMG after being laser processed with various parameters.

Scan speed	30 mm/s	200 mm/s	300 mm/s
UV laser, 6 J/cm^2	~30 μm	~11.2 μm	~7.2 μm
UV laser, 12 J/cm^2	~80 μm	~15.2 μm	~8.8 μm
IR laser, 9.5 J/cm^2	0 μm	–	–
IR laser, 19 J/cm^2	~0.9 μm	0 μm	–

The laser power affects the micromachining depth at a given scan speed; the cutting depth increases with increasing laser power and decreasing scan speed. In addition, the wavelength is a key parameter in the machining of Mg-based BMG specimens. For the IR laser with a fluence of 19 J/cm^2 and a scan speed of 30 mm/s, the cutting depth was only ~0.9 μm.

Fig. 2 shows the top and cross-sectional views of the laser-machined Mg-based BMG specimens obtained with various laser sources, irradiation energies, and scan speeds. The surface morphology of a groove machined using the UV laser with a fluence of 12 J/cm^2 and a scan speed of 30 mm/s is characterized by small ridges with a height of 50 μm on either side of the groove, as shown in Fig. 2(a) and (d). A large number of re-deposited materials or particles are observed between the ridges close to the groove; outside of the ridges, away from the groove, a number of wrinkles appear after plastic deformation. This phenomenon implied that the inner region between the ridges contained some deposited materials due to plasma cloud induced by the UV laser irradiation of 12 J/cm^2, and the HAZ, outside of the irradiated area, exhibited plastic wrinkles due to heat accumulation caused by a slow scan speed of 30 mm/s. The heat accumulation and thermal diffusion has the effect of softening the materials located within the HAZ because of temperatures exceeding the temperature T_g. On the other hand, the materials within the irradiated region undergo melting and vaporization to generate volume expansion. Plastic deformation is induced in the soft HAZ owing to the volume expansion of the irradiated region. When the scan speed was increased to 200 mm/s or above, the HAZ became smaller due to faster thermal dissipation, and the deformed wrinkles decreased in number or disappeared. The sprayed materials on either side of the machined grooves are shown in Fig. 2(b) and (e).

No groove is produced in the surface of the Mg-based BMG specimens when the IR laser with a fluence of 19 J/cm^2 and a scan rate of 30 mm/s was used (Fig. 2(c) and (f)). Under these conditions, the surface was heated to achieve viscous flow (over the temperature T_g). It is suggested that the thermal heating and penetration effects of the IR laser (wavelength of 1064 nm) do not induce the ablation effect via material spray, even if a fluence of

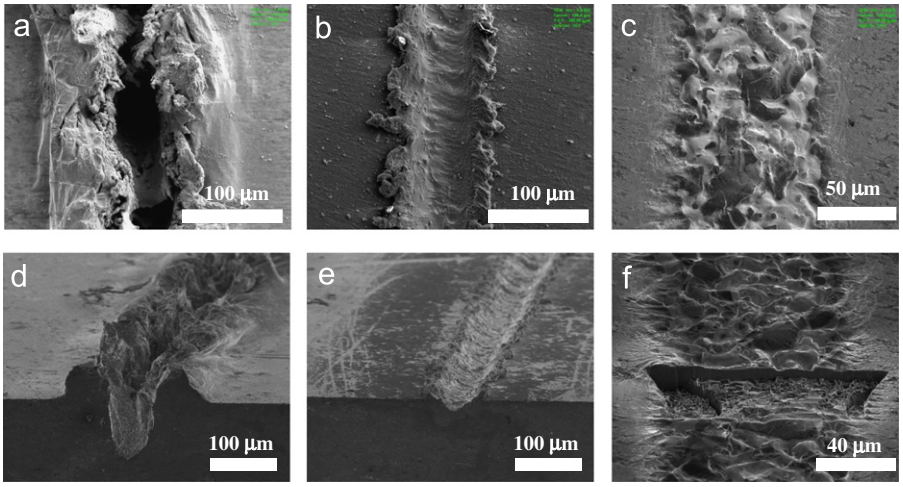

Fig. 2. Top view and cross-sectional view of Mg-based BMG after laser micromachining with (a) and (d) a UV laser with a fluence of 12 J/cm^2 and a scan speed of 30 mm/s, (b) and (e) a UV laser with a fluence of 12 J/cm^2 and a scan speed of 300 mm/s, and (c) and (f) an IR laser with a fluence of 19 J/cm^2 and a scan speed of 30 mm/s.

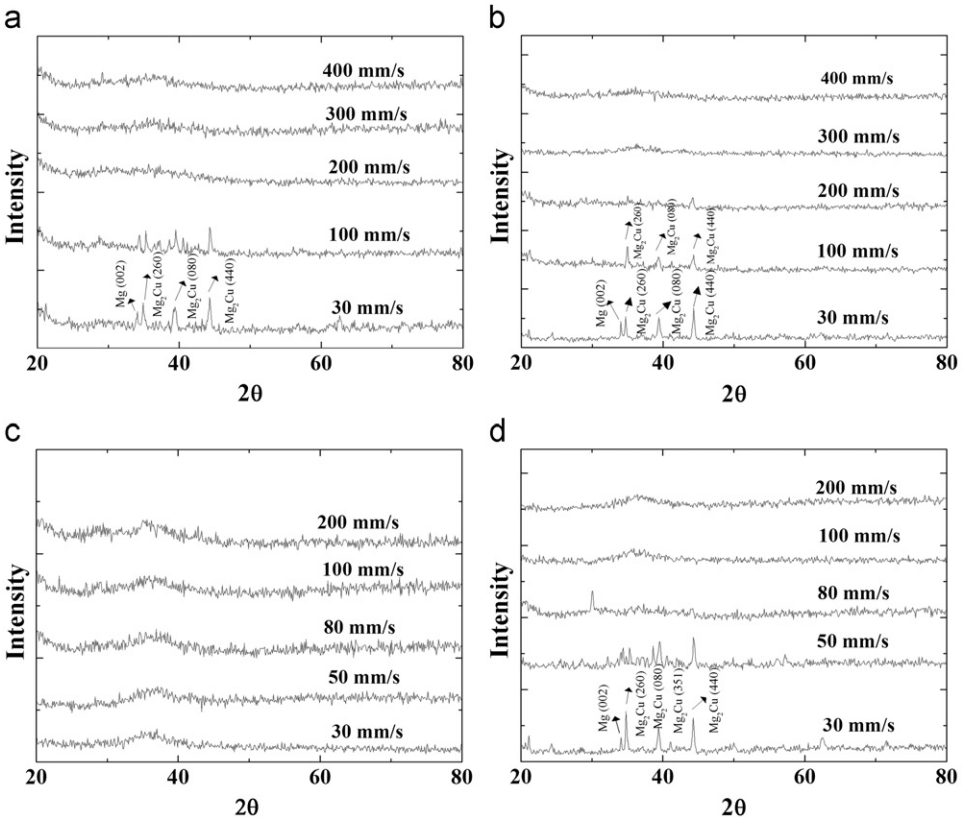

Fig. 3. XRD patterns of specimens obtained using (a) a UV laser with a fluence of 6 J/cm^2, (b) a UV laser with a fluence of 12 J/cm^2, (c) an IR laser with a fluence of 9.5 J/cm^2, and (d) an IR laser with a fluence of 19 J/cm^2 at various scan speeds.

19 J/cm^2 and a slow scan speed of 30 mm/s are used. Therefore, the absorption of laser light is a crucial factor for the machining of Mg-based BMGs. The good absorption rate of short-wavelength irradiation produced by the UV laser by the Mg-based BMG makes this laser very suitable for machining. To minimize the HAZ and to achieve uniform cutting, a fast scan speed (e.g., 300 mm/s) appears to be appropriate.

To investigate where there is any crystalline structure induced in the Mg-based BMG specimens after the laser process, BMG disks were scanned with one pass of the laser with a spacing of 70 μm for XRD analysis. Fig. 3 shows the XRD patterns of the BMG specimens after laser cutting at various laser powers and scan speeds. For the UV laser with a lower fluence of 6 J/cm^2, the critical speed of crystalline transformation was 100 mm/s, as shown in Fig. 3(a). With a higher fluence of 12 J/cm^2, the Mg-based BMG specimens were readily transformed into a crystalline phase of Mg_2Cu and pure Mg after cutting by the UV laser at scan speeds below 200 mm/s, as shown in Fig. 3(b). For the 1064 nm IR laser with a fluence of 9.5 J/cm^2, all specimens exhibited the amorphous phase independent of the scan speed, as shown in Fig. 3(c). However, at a higher fluence of 19 J/cm^2, the Mg-based amorphous phase remained intact for scan speeds of 100 mm/s or faster, as shown in Fig. 3(d). During these laser cutting experiments, transformation of the Mg-based BMG into a crystalline

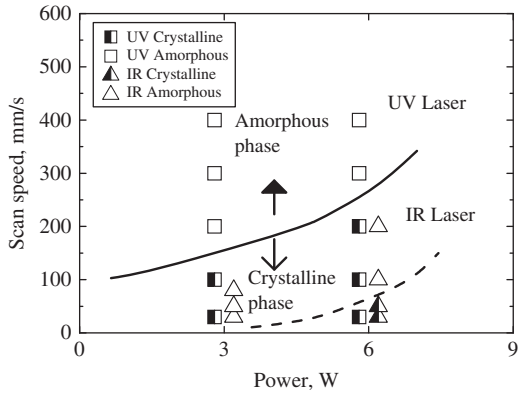

Fig. 4. Phase transformation summary of Mg-based BMG after laser scanning at various wavelengths and with various processing parameters.

phase occurred more readily with increasing laser fluence and decreasing scan speed for both laser wavelengths.

Fig. 4 shows a summary of the phase transformation behavior of the Mg-based BMG after laser cutting at various wavelengths and laser powers. Regions with amorphous and crystalline phases are defined based on the current results. The data illustrate that the amorphous nature of BMG specimens is more likely to be retained when a low laser power and high scan speed are used. Transformation into a crystalline phase(s) occurs at high power and a low scan speed. BMG materials are more prone to crystallization under irradiation with a shorter laser wavelength for a given set of operating conditions. Because the photon energy of a short wavelength is higher than that of a long wavelength at a given laser power, the 355 nm wavelength has more energy to affect the material than that of the 1064 nm wavelength laser. Furthermore, the absorption of the 355 nm irradiation by the Mg-based BMG was higher than the absorption of the 1064 nm laser, thereby providing more energy for cutting the BMG material.

Based on these results, the cutting depth of Mg-based BMG is around 8.8 μm for laser machining using a 355 nm laser with a fluence of 12 J/cm^2 and a scan speed of 300 mm/s. With an appropriate laser power and scan speed, the amorphous phase of Mg-based BMG can be maintained after the laser machining process. The laser process is thus suitable for machining of BMG materials.

4. Conclusion

Pulsed lasers were used to micromachine Mg-based bulk metallic glass (BMG), with cutting depths of 1–80 μm. Mg-based BMG exhibited a better absorption rate and higher photon energy with the 355 nm UV laser than with the 1064 nm IR laser. The amorphous phase of the Mg-based BMG was preserved for scan speeds exceeding 200 mm/s. Effective micromachining of Mg-based BMG can be achieved using a UV laser with a fluence of 12 J/cm^2 and a scan speed of 300 mm/s while maintaining its amorphous structure. Due to the lower rate of absorption by Mg-based BMG, the IR laser is not suitable for the micromachining process.

Acknowledgment

Dr. C.J. Lee gratefully acknowledges the financial support from the National Science Council of Taiwan, R.O.C., under grants NSC 99–2811-E-110-006 and NSC 99–2818-E-110-002.

References

[1] Ashby MF, Greer AL. Metallic glasses as structural materials. Scr. Mater. 2006;54:321–6.
[2] Schroers J, Nguyen T, O'Keeffe S, Desai A. Thermoplastic forming of bulk metallic glass—Applications for MEMS and microstructure fabrication. Mater. Sci. Eng.: A-Struct. Mater. Prop. Microstruct. Process 2007;449:898–902.
[3] Kumar G, Tang HX, Schroers J. Nanomoulding with amorphous metals. Nature 2009;457:868–72.
[4] Sun H, Flores KM. Microstructural analysis of a laser-processed Zr-based bulk metallic glass. Metall. Mater. Trans.: A-Phys. Metall. Mater. Sci. 2010;41A: 1752–7.
[5] Bakkal M, Shih AJ, Scattergood RO. Chip formation, cutting forces, and tool wear in turning of Zr-based bulk metallic glass. Int. J. Mach. Tools Manuf. 2004;44:915–25.
[6] Bakkal M, Shih AJ, McSpadden SB, Liu CT, Scattergood RO. Light emission, chip morphology, and burr formation in drilling the bulk metallic glass. Int. J. Mach. Tools Manuf. 2005;45:741–52.
[7] Li WX, Minev R, Dimov S, Lalev G. Patterning of amorphous and polycrystalline Ni(78)B(14)Si(8) with a focused-ion-beam. Appl. Surf. Sci. 2007;253: 5404–10.
[8] Slocombe A, Li L. Laser ablation machining of metal/polymer composite materials. Appl. Surf. Sci. 2000;154:617–21.
[9] Atanasov PA, Eugenieva ED, Nedialkov NN. Laser drilling of silicon nitride and alumina ceramics: a numerical and experimental study. J. Appl. Phys. 2001;89:2013–6.
[10] Jia W, Peng ZN, Wang ZJ, Ni XC, Wang CY. The effect of femtosecond laser micromachining on the surface characteristics and subsurface microstructure of amorphous FeCuNbSiB alloy. Appl. Surf. Sci. 2006;253:1299–303.
[11] Shanjin L, Yang W. An investigation of pulsed laser cutting of titanium alloy sheet. Opt. Lasers Eng. 2006;44:1067–77.
[12] Wang XL, Lu PX, Dai NL, Li YH, Liao CR, Zheng QG, et al. Noncrystalline micromachining of amorphous alloys using femtosecond laser pulses. Mater. Lett. 2007;61:4290–3.
[13] Quintana I, Dobrev T, Aranzabe A, Lalev G, Dimov S. Investigation of amorphous and crystalline Ni alloys response to machining with micro-second and pico-second lasers. Appl. Surf. Sci. 2009;255:6641–6.
[14] Wang HS, Chen HG, Jang JSC, Chiou MS. Combination of a Nd:YAG laser and a liquid cooling device to (Zr(53)Cu(30)Ni(9)Al(8))Si(0.5) bulk metallic glass welding. Mater. Sci. Eng.: A-Struct. Mate.r Prop. Microstruct. Process 2010;528:338–41.
[15] Ma FX, Yang JJ, Zhu XN, Liang CY, Wang HS. Femtosecond laser-induced concentric ring microstructures on Zr-based metallic glass. Appl. Surf. Sci. 2010;256:3653–60.
[16] Schroers J, Lohwongwatana B, Johnson WL, Peker A. Gold based bulk metallic glass. Appl. Phys. Lett. 2005;87:061912.
[17] Pan CT, Wu TT, Chen MF, Chang YC, Lee CJ, Huang JC. Hot embossing of micro-lens array on bulk metallic glass. Sens. Actuator A-Phys. 2008;141: 422–31.
[18] Chang YC, Wu TT, Chen MF, Lee CJ, Huang JC, Pan CT. Finite element simulation of micro-imprinting in Mg-Cu-Y amorphous alloy. Mater. Sci. Eng. A-Struct. Mater. Prop. Microstruct. Process 2009;499:153–6.
[19] Chu JP, Chiang CL, Wijaya H, Huang RT, Wu CW, Zhang B, et al. Compressive deformation of a bulk Ce-based metallic glass. Scr. Mater. 2006;55:227–30.